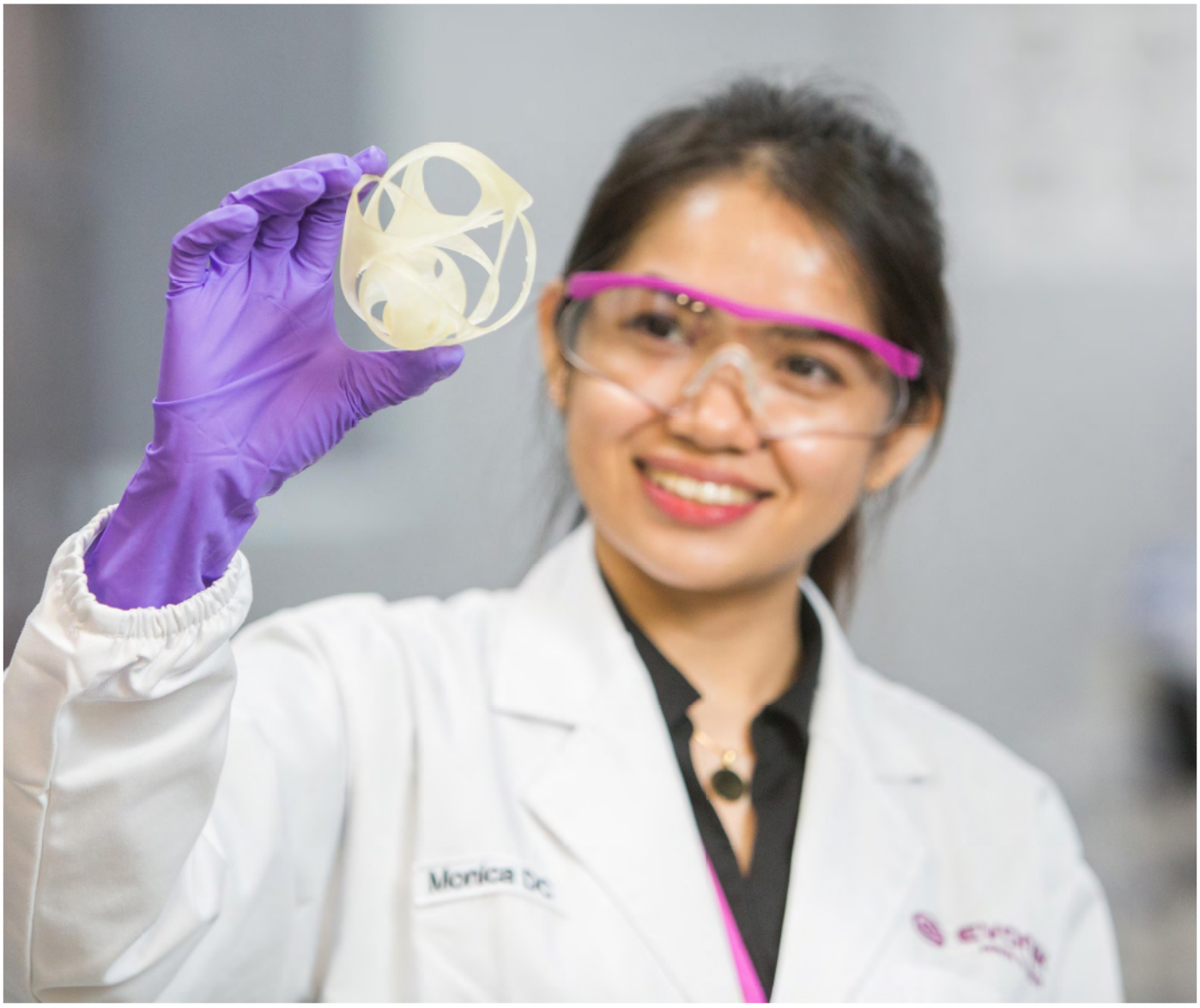

Pushing the boundaries of chemistry? It takes #HumanChemistry

Make your curiosity and talent as a chemist matter to the world with a specialty chemicals leader. Together, we combine cutting-edge science with engineering expertise to create solutions that answer real-world problems. Find out how our approach to technology creates more opportunities for growth, and see what chemistry can do for you at:

evonik.com/career

EVONIK
Leading Beyond Chemistry

ADVANCED FUNCTIONAL MATERIALS
www.afm-journal.de

Transient Rechargeable Battery with a High Lithium Transport Number Cellulosic Separator

Neeru Mittal, Alazne Ojanguren, Nicola Cavasin, Erlantz Lizundia, and Markus Niederberger**

Transient batteries play a pivotal role in the development of fully autonomous transient devices, which are designed to degrade after a period of stable operation. Here, a new transient separator-electrolyte pair is introduced for lithium ion batteries. Cellulose nanocrystals (CNCs) are selectively located onto the nanopores of polyvinyl alcohol membranes, providing mobile ions to interact with the liquid electrolyte. After lithiation of CNCs, membranes with electrolyte uptake of 510 wt%, ionic conductivities of 3.077 $mS \cdot cm^{-1}$, electrochemical stability of 5.5 V versus Li/Li^+, and high Li^+ transport numbers are achieved. Using an organic electrolyte, the separators enable stable Li metal deposition with no dendrite growth, delivering 94 $mAh \cdot g^{-1}$ in $Li/LiFePO_4$ cells at 100 $mA \cdot g^{-1}$ after 200 cycles. To make the separator-electrolyte pair transient and non-toxic, the organic electrolyte is replaced by a biocompatible ionic liquid. As a proof of concept, a fully transient Li/V_2O_5 cell is assembled, delivering 55 $mAh \cdot g^{-1}$ after 200 cycles at 100 $mA \cdot g^{-1}$. Thanks to the reversible Li plating/stripping, dendrite growth suppression, capacity retention, and degradability, these materials hold a bright future in the uptake of circular economy concepts applied to the energy storage field.

1. Introduction

Transient technology is a flourishing area of research aimed at designing materials and devices that undergo controlled degradation processes after a period of stable and reliable operation.[1,2] Transient energy storage systems such as batteries may enable fully autonomous and self-sufficient transient electronic devices that do not rely on external power sources.[3] Transient batteries have the ability to disintegrate, dissolve, or be resorbed or degraded at the end of their life. Accordingly, transient batteries have a high potential to reduce the environmental footprint caused by inadequate disposal of used lithium ion batteries (LIBs), which leads to large amounts of hazardous materials in the environment.[4] Preventing the accumulation of durable and potentially harmful materials in marine, river, and land environments is an imperative task to protect "Life below water" and "Life on land" as part of the Sustainable Development Goals of the United Nations.[5]

The separator-electrolyte pair plays a key role in the pursuit of high energy density and safe LIBs as they must ensure an efficient and safe ion transport between the anode and cathode during discharge/charge.[6] Conventional separator-electrolyte pairs consist of a porous petroleum-based membrane (polypropylene, polyethylene...) soaked into an organic solvent (ethylene carbonate (EC), dimethyl carbonate (DMC)...) containing dissolved lithium salts.[7] As neither these separators nor organic solvents are transient or biocompatible, transient batteries require novel separator-electrolyte pairs with efficient Li^+ transport and degradation on demand.[8,9]

A step forward toward safer and longer-lasting batteries may arise from the suppression of the needle-like Li dendrite formation, which reduces the amount of active Li and eventually leads to short-circuit and associated fire or explosion hazards.[10] Dendritic Li metal deposition can be limited by suppressing the competitive transport of Li^+ ions and counteranions in the electrolyte used. Notable efforts have been done to develop high Li^+ transport unit (t_{Li^+}) electrolytes as they can suppress the counteranion transport.[11] Among different alternatives, polymeric conductors are of special interest because they combine the inherent good processability of polymers together with a wide operational voltage window and relatively high ionic conductivities.[12,13] Many of the ionic conductors with high Li^+ transport

N. Mittal, A. Ojanguren, N. Cavasin, Prof. M. Niederberger
Laboratory for Multifunctional Materials
Department of Materials
ETH Zürich
Vladimir-Prelog-Weg 5, Zurich 8093, Switzerland
E-mail: markus.niederberger@mat.ethz.ch
Dr. E. Lizundia
Life Cycle Thinking Group
Department of Graphic Design and Engineering Projects
Faculty of Engineering in Bilbao
University of the Basque Country (UPV/EHU)
Bilbao 48013, Spain
E-mail: erlantz.liizundia@ehu.eus
Dr. E. Lizundia
BCMaterials
Basque Center for Materials
Applications and Nanostructures
UPV/EHU Science Park, Leioa 48940, Spain

The ORCID identification number(s) for the author(s) of this article can be found under https://doi.org/10.1002/adfm.202101827.

DOI: 10.1002/adfm.202101827

numbers rely on poly(ethylene oxide).[14] Although poly(ethylene oxide) has been used in LIBs since the 1970s, its ability to protect the battery against dendrite puncture is limited,[15] and batteries with long lifespan are difficult to achieve when applied in high-voltage (>4 V) cathodes given the low oxidative stability of its ether groups.[16]

Upon lithiation, cellulose nanocrystals (CNC-Li; lithiated cellulose nanocrystals) provide an adequate platform for the development of Li^+ conductors with a remarkable t_{Li}^+ of 0.93 and a wide operational window.[17] CNCs are extracted through a controlled sulfuric acid-induced cleavage of the glycosidic bonds of cellulose to yield 5–10 nm wide and 100–1000 nm long anisotropic nanoparticles, decorated with hydroxyl (-OH) and anionic sulfate half-ester groups ($-OSO_3^-$).[18] The β-1,4-linked anhydro-D-glucose chains in CNCs are packed into a monoclinic structure with two chains per unit cell, forming nanoscale rods with crystallinity values exceeding 85–90%.[18] As a result, CNCs show a specific modulus (Young's modulus to weight ratio) of 85 $J \cdot g^{-1}$ (versus 25 for steel),[18] making them highly resistant against dendrites. Cellulosic nanoparticles have already shown good properties for energy storage applications,[19,20] and given their non-toxic character emerge as good candidates to develop transient devices.

To improve the electrode-electrolyte interface and achieve long-term stable cycling, CNCs can be embedded within a mechanically soft and ductile matrix which accommodates the electrode expansion/shrinkage during Li^+ intercalation/deintercalation.[21] Poly(vinyl alcohol) (PVA) is a perfect match as it is a prominent example of a water-soluble polymer (thus highly compatible with CNCs) with easy processing and stiff but ductile character (tensile strength: 52 MPa, elongation at break: 150%).[22] To date, PVA has been proven as an adequate separator for conventional LIBs thanks to its good chemical and thermal resistance, high electrolyte wettability, and electrochemical stability against Li/Li^+.[23,24] It is our hypothesis that a separator consisting of CNC-Li and PVA may be easily disintegrated once the proper trigger (aqueous solution) is applied.

The temperature stability of LIBs is a critical safety feature. When batteries are exposed to high external temperatures or experience an internal temperature rise, conventional polyolefin separators like Celgard start to shrink, strongly increasing the risk of short-circuits, battery failures, and explosion events.[25] Accordingly, the development of membranes with good mechanical integrity at high temperatures can reduce the likelihood of thermal runaway,[26] which ensures good battery safety by providing reliable electrical insulation between battery electrodes even at high temperatures.[7] In contrast to the melting temperature of Celgard, which is <160 °C, PVA and CNCs have a high melting temperature of 222 °C[27] and an onset of thermal degradation of 250 °C,[28] respectively, making the PVA/CNC pair an appropriate candidate for the development of battery separators with good thermal stability.

While a prevailing Li^+ transport is achieved upon lithiation, the separator's ionic conductivity is boosted via infusion of a liquid phase that offers enhanced Li^+ mobility.[7,29] Conventional LIBs use organic solvent-based liquid electrolytes, representing a serious limitation toward transiency due to their flammability, safety issues, and toxicity. Therefore, a transient and non-toxic alternative should be implemented for secondary transient batteries. Ionic liquids (ILs) are molten salts composed of positive and negative charges with reasonable ionic conductivity and a wide electrochemical potential stability window.[30] ILs can provide an enhanced Li^+ transport number as a result of anion coordination, supporting a long-term stable Li-metal deposition.[31] Despite all the advantages, to date no works have applied ILs into secondary transient batteries as their use has mainly been limited to degradable primary Mg batteries,[32] or supercapacitors.[33]

In this work we design a transient high transport number Li^+ conductor for degradable LIBs. Porous membranes comprising a PVA matrix with embedded CNCs are obtained through non-solvent induced phase separation (NIPS) method. Lithiated CNCs are incorporated to enhance the Li^+ transport number and ionic conductivity, delivering 94 $mAh \cdot g^{-1}$ after 200 cycles in secondary $Li/LiFePO_4$ cells (18 $mAh \cdot g^{-1}$ for Celgard). The as-obtained separator enables stable Li plating and stripping and steady operation in $Li/LiFePO_4$ cells. Moreover, a biocompatible IL is infused within the porous separator to form a fully degradable, green, and sustainable LIB separator. The IL soaked transient separator is finally assembled into a fully transient Li/V_2O_5 battery that delivers 55 $mAh \cdot g^{-1}$ after 200 cycles and disintegrates in an aqueous solution within 15 min, providing a proof of concept for the applicability of PVA/CNC-Li membranes for transient energy storage devices. The stable Li metal deposition with a highly reversible voltage response, small over-potential, and no Li dendrite growth make PVA/CNC-Li membranes also attractive for non-transient conventional LIBs, enabling longer cycle life batteries.

2. Results and Discussion

2.1. CNC Lithiation

The lithiation of CNC is studied by attenuated total reflectance-Fourier transform infrared (ATR–FTIR) and X-ray diffraction (XRD). FTIR spectra in **Figure 1**a shows the characteristic absorption peaks corresponding to cellulose, with a broad band in the 3650–3200 cm^{-1} region due to the O—H stretching, and narrower bands at 2902 cm^{-1} (asymmetric and symmetric C—H stretching), 1337 cm^{-1} (C—O—H bending), 1160 cm^{-1} (C—O—C bending), 897 cm^{-1} (C—O—C asymmetric stretching). The bands at 1110 and 980 cm^{-1} indicate the presence of $-OSO_3^-$ as a result of the sulfuric acid-induced hydrolysis conducted during CNC isolation from cellulose. A change in the intra- and intermolecular bonds of cellulose is suggested by the intensity decrease and shift of the bands at 1236 and 1202 cm^{-1} to 1239 and 1207 cm^{-1}, respectively.[34] As those absorption bands are assigned to the δCOH in plane at C6 (carbon atoms of the glucose unit of cellulose),[34] it is suggested that the primary hydroxyl groups at the C6 position are successfully exchanged with Li^+ during alkali treatment of CNCs with LiOH. As displayed in Figure 1b, bare CNCs show the characteristic diffraction peaks of cellulose I corresponding to (101), (10-1), (200), and (004) planes at 2θ = 14.9, 16.5, 22.7, and 34.4°. A new peak corresponding to cellulose II appears at 2θ = 12.1° after LiOH treatment, indicating a transformation from cellulose I to cellulose II upon lithiation. Such coexistence of cellulose I and cellulose II phases in CNC-Li occurs as a result of the intracrystalline swelling in concentrated aqueous LiOH, similar to the mercerization reaction occurring in NaOH solution.

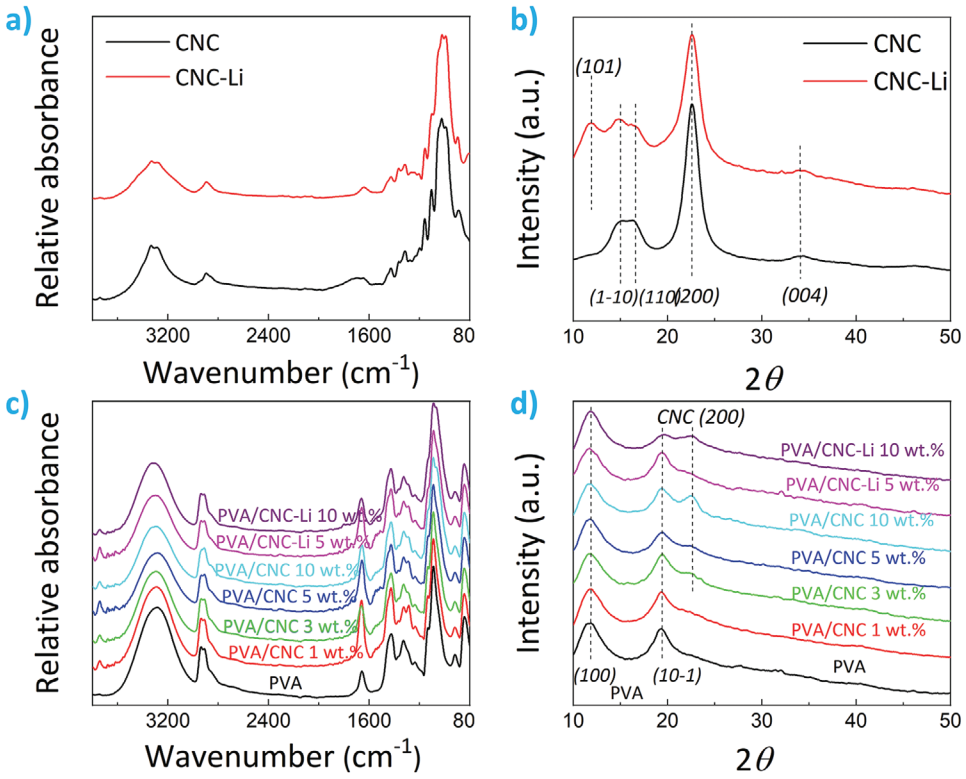

Figure 1. CNC lithiation characterization: a) ATR–FTIR spectra and b) XRD patterns of original and lithiated CNCs. Membrane characterization: c) ATR–FTIR spectra and d) XRD patterns of bare PVA, PVA/CNC, and PVA/CNC-Li membranes at different concentrations.

ATR–FTIR experiments are also performed on PVA/CNC and PVA/CNC-Li membranes. As shown in Figure 1c, the neat PVA membrane presents a pronounced hydroxyl stretching region at 3600–3000 cm^{-1}, with further bands at 2917, 1690, 1425, 1324, 1081, and 839 cm^{-1} originating from CH_2 asymmetric stretching, C=O carbonyl stretching, CH_2 bending, C–H deformation, C–O stretching and C–C stretching, respectively.[35] No traces of polyvinylpyrrolidone (PVP) are observed in the PVA separators (Figure S2, Supporting Information). A new shoulder at 1160 cm^{-1} is observed for samples containing CNCs due to the C–O–C bending of cellulose. The –OH peak centered at 3285 cm^{-1} is shifted to 3320 cm^{-1}, suggesting hydrogen bonds between the PVA matrix and CNCs. Interestingly, the well-defined peak at 1144 cm^{-1} for neat PVA is smoothed after CNC (or CNC-Li) incorporation, indicating a lower degree of crystallinity. XRD patterns in Figure 1d show two main diffraction peaks at $2\theta = 11.5$ and 19.4° arising from the (100) and (10-1) planes of PVA, which remain superimposed over an amorphous halo.[36] This predominantly amorphous character of prepared membranes proves favorable for enhancing the Li^+ transport across the separator.[6]

2.2. Membrane Morphological Characterization

In this work we aim at fabricating porous LIB separators with transient ability. PVA is selected as a water-soluble model polymer with adequate chemical/thermal resistance, high electrolyte affinity, and electrochemical stability.[23,24] CNCs are incorporated into PVA to improve the ionic conductivity. Free-standing, centimeter-sized porous membranes are fabricated via a wet process involving NIPS (Figure S3, Supporting Information). **Figure 2** shows the top-view SEM images of the PVA/CNC membranes with different concentrations of CNCs and CNC-Li, while Figure S4, Supporting Information, presents the corresponding cross-sectional SEM images. Neat PVA shows homogeneously distributed pores whose sizes vary from roughly 2 to 4 µm. They are formed upon PVP dissolution into the ethanol bath from the PVA/PVP membrane. The images in Figure 2c–e reveal that the size of the pores continuously decreases after CNC incorporation, with pore sizes in the range of 0.5–1.2 µm for the membrane containing 10 wt% of CNCs. As depicted in Figure 2f,g, a similar effect is obtained in the presence of lithiated CNCs, resulting in PVA membranes with homogeneously distributed small pores. Importantly, the CNCs are exposed to the outside medium as they remain preferentially located on the surface of the pores (Figure S5, Supporting Information). This effect is achieved because CNCs migrate to the PVA/PVP interface as a solid emulsifier, stabilizing the solution.[37] Such selective localization increases the interaction of CNC surface with the liquid electrolyte, thus providing a large amount of mobile Li^+ (from the $-OSO_3Li$ groups present on lithiated CNCs) at low weight CNC-Li concentrations within the nanocomposite membrane. As a result, we expect to obtain large ionic conductivities upon soaking these membranes in liquids that are able to act as Li^+ transport medium.[17] The role

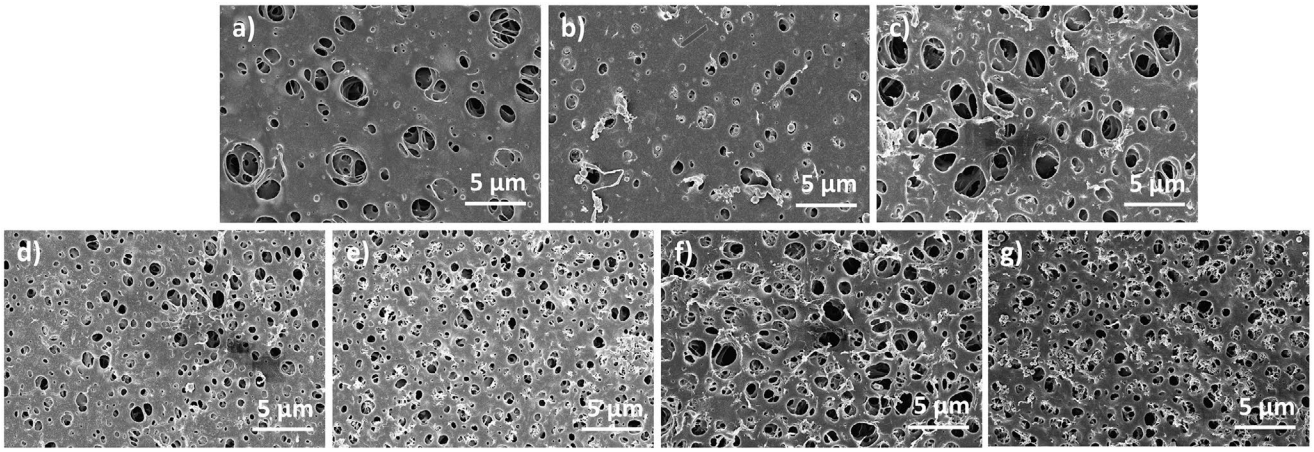

Figure 2. Representative SEM micrographs showing the top-view onto the PVA/CNC membranes obtained upon non-solvent induced phase separation: a) neat PVA; b) PVA/CNC 1 wt%; c) PVA/CNC 3 wt%; d) PVA/CNC 5 wt%; e) PVA/CNC 10 wt%; f) PVA/CNC-Li 5 wt%; and g) PVA/CNC-Li 10 wt%.

of CNC as an efficient emulsifier reduces the size of the dispersed PVP phase with increasing concentration, resulting in membranes with more, but smaller pores, which is beneficial for uniform ion transport across the electrodes and limitation of Li dendrite growth.[38]

2.3. Thermal Stability

To assess the potential of PVA/CNC separators to protect the battery from thermal runaway at high-temperatures,[26] the thermal stability of our membranes was studied by thermogravimetric analysis (TGA) and dimensional stability measurements at 160 °C. **Figure 3**a shows the TGA curves of PVA-based membranes, while Figure 3b displays the weight loss rate obtained as the first derivative of the weight with respect to temperature. The pure PVA membrane shows a smooth weight loss at ≈45 °C due to moisture evaporation followed by two degradation stages centered at 310 and 490 °C due to chain scission events in PVA.[39] Upon CNC incorporation, the onset of thermal degradation (the temperature at which the first 5 wt% loss is observed) decreases from 244 °C for neat PVA to 223 and 225 °C for PVA/CNC 10 wt% and PVA/CNC-Li 10 wt% membranes, respectively. In spite of the slightly reduced thermal stability after CNC addition, the composite membranes show acceptable thermal stabilities within the expected operating temperature range of LIBs.

As shown in Figure 3c, the Celgard membrane suffers significantly when it is heated to 160 °C. Due to the melting of polymeric crystals leading to the release of the internal shrink force,[40] the Celgard separator shrinks (defined as the area reduction) by ≈48% after 60 min, while it is completely melted after 120 min. Conversely, the neat PVA membrane keeps its shape rather unchanged with a shrinkage as low as 2% after 120 min at 160 °C. However, it slightly turns yellowish due to the thermodegradation events occurring at macromolecular

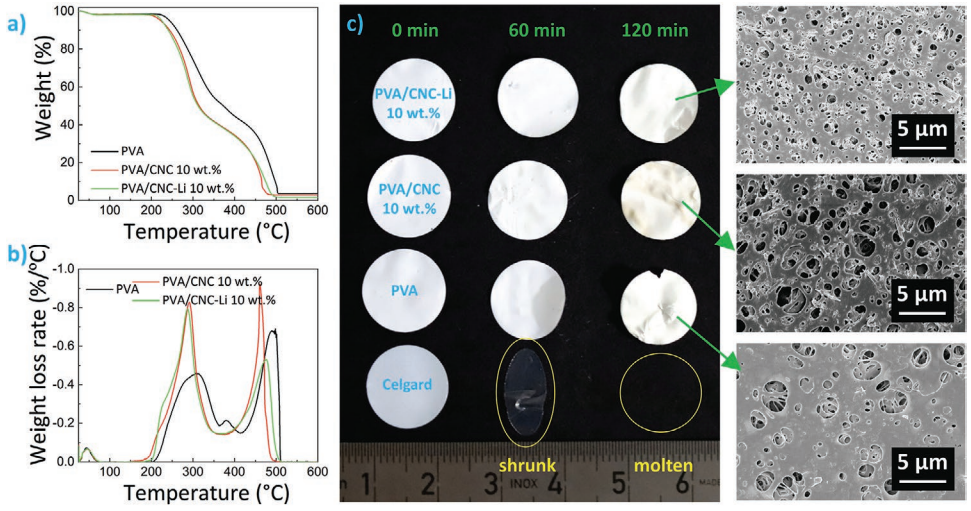

Figure 3. Thermal stability of PVA/CNC-Li membranes: a) Thermogravimetric traces and b) weight loss rates at 10 °C·min^{-1} under air atmosphere. c) Optical photographs obtained after maintaining the membranes at 160 °C in an oven for 0, 60, and 120 min. Representative SEM micrographs of the membranes obtained after thermal treatment at 160 °C for 120 min.

level. Interestingly, the presence of both CNC and CNC-Li completely suppresses the thermal shrinkage of the membrane and also reduces the yellowing effect (note that PVA/CNC still presents a slight yellowish effect, while PVA/CNC-Li remains white), indicating their superior stability at high temperatures in comparison with separators based on pure petrochemical resources. The H-bonding between PVA and the hydroxyl groups of CNCs inhibits unzipping or depolymerization of PVA,[39] resulting in membranes that are able to keep their porous morphology virtually unchanged as proven by the SEM images on the right part of Figure 3c. Moreover, the 3D structure provided by CNCs acts as a heat and mass barrier, limiting the elimination of volatile products (saturated and unsaturated aldehydes and ketones) arising from PVA thermodegradation.

2.4. Organic Electrolyte-Soaked Membranes

Ideally, a battery separator should exhibit a large electrolyte uptake (EU) capacity so as to ensure adequate compatibility with the ion-conducting media.[6] Accordingly, the EU of different membranes (Equation S1, Supporting Information) is summarized in **Figure 4**a. Thanks to the lyophilic character of cellulose, membranes with higher CNC concentrations show larger EU values as denoted by the increase from 245.7% for pure PVA to 360.7% for the PVA/CNC 10 wt% membrane. More importantly, for a given CNC concentration, lithiated CNCs prove to be more efficient in increasing the EU, reaching a maximum of 509.1% for PVA/CNC-Li 10 wt% membrane. Such remarkably large EU values can be explained by both the enhanced membrane-electrolyte compatibility provided by the lithiation step and the higher porosity provided by CNCs. Indeed, Figure S6, Supporting Information shows the N_2 adsorption-desorption isotherms of PVA and PVA/CNC membranes, which are characterized by a type IV isotherm with H_2 hysteresis. Such curve shape suggests the presence of mesopores to yield Brunauer–Emmett–Teller surface areas of 66.9, 66.5, and 57.9 $m^2 \cdot g^{-1}$ for PVA, PVA/CNC, and PVA/CNC-Li, respectively. The high surface areas in comparison with commercial membranes (11 $m^2 \cdot g^{-1}$ for glass microfiber and 41 $m^2 \cdot g^{-1}$ for Celgard)[41] are beneficial for battery applications as they may lead to additional pathways for Li^+ diffusion.[6]

As shown in Figure 4b, the improved electrolyte affinity provided by lithiated CNCs is translated into an enhanced Li^+ conductivity σ_i, which is obtained according to Equation S2, Supporting Information from the Nyquist impedance plots shown in Figure S7, Supporting Information. In such system, the liquid electrolyte provides a transport medium for the mobile Li^+ arising from the surface $-OSO_3Li$ groups on lithiated CNCs,[17] and the 3D porosity imparts efficient and short paths for Li^+ migration, yielding a maximum conductivity of 3.077 $mS \cdot cm^{-1}$ for the PVA/CNC-Li 10 wt% membrane (see Table S2, Supporting Information for further details). Such conductivity value is larger than the 0.508 $mS \cdot cm^{-1}$ obtained for the commercial Celgard separator, and also surpasses the conductivity values reported for several other LIB separators based on cellulose nanofibers (0.75 $mS \cdot cm^{-1}$),[42] agarose (0.87 $mS \cdot cm^{-1}$),[43] or cyanoethyl-chitin nanofiber (0.45 $mS \cdot cm^{-1}$).[44]

Our group has demonstrated that CNC lithiation can yield membranes, which efficiently prevent ion concentration

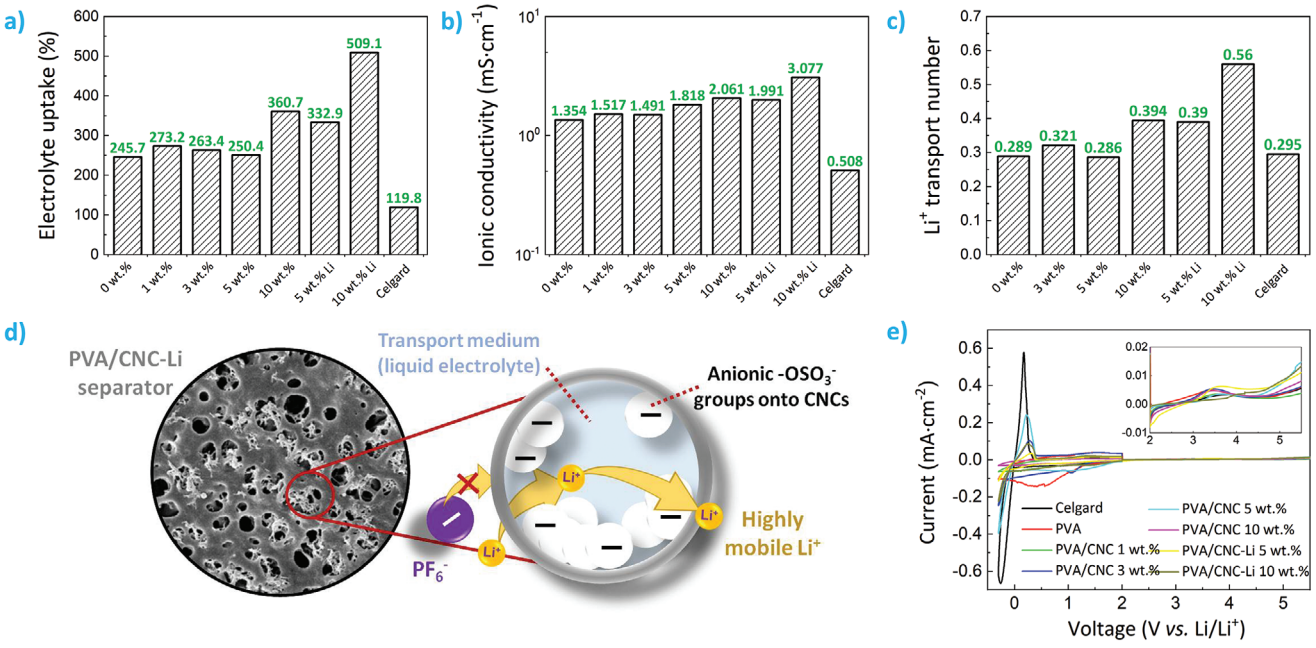

Figure 4. a) Electrolyte uptake; b) ionic conductivity; and c) Li^+ transport number of PVA/CNC membranes soaked in 1 M $LiPF_6$ in DMC/EC (50:50 vol.) electrolyte. d) SEM image and schematic illustration of the proposed Li^+ conduction mechanism within the porous PVA/CNC-Li membrane; and e) electrochemical stability window of the membranes obtained through a combination of cyclic voltammetry (–0.3 to 2.0 V) and linear sweep voltammetry (2.0 to 5.5 V) recorded at 1 $mV \cdot s^{-1}$ with a stainless steel working electrode and a metallic Li counter electrode. The inset shows the magnification of the region between 2.0 to 5.5 V.

gradients and enable stable alkali metal deposition.[17] Accordingly, Figure 4c shows the Li^+ transport number (t_{Li}^+) determined by the Bruce–Vincent method (Equation S3, Supporting Information).[45] Current-time profiles and impedance spectra obtained before and after the voltage polarization of a symmetric Li/Li cell shown in Figure S8, Supporting Information were used for t_{Li}^+ determination.[45] t_{Li}^+ is defined as transport number to distinguish the obtained values from the Li^+ transference number, which is usually calculated in polymer electrolytes by the Bruce–Vincent method, provided there is no ion association (in agreement with the Nernst–Einstein equation).[46–48] In the case of concentrated electrolytes (exceeding 0.01 M), however, the application of the Bruce–Vincent method can overestimate the true transference number,[47,49] so the term transport number may be more accurate.[48] As shown in Figure 4c, t_{Li}^+ increases with CNC concentration until reaching a maximum of $t_{Li}^+ = 0.56$ for the PVA/CNC-Li 10 wt% membrane. In comparison, in PVA/CNC 10 wt% the Li^+ transport number is 0.394, and for bare PVA and Celgard, it is calculated to be 0.289 and 0.295, respectively. The increase in σ_i and t_{Li}^+ values upon CNC-Li addition indicates that Li^+ motion through the porous separator-electrolyte pair is boosted by the dissociation of the weakly associated Li^+ ions from the $-OSO_3Li$ groups located on the surface of CNC-Li, as schematically shown in Figure 4d.

Apart from ensuring an efficient ion conduction and electrical insulation between electrodes, the separator membranes must also be electrochemically stable in a wide voltage window to avoid unwanted side reactions arising from electrolyte decomposition.[50] Figure 4e displays a combined cyclic and linear sweep voltammogram in the −0.2 to 5.5 voltage (versus Li/Li^+) range. The voltage stability of Celgard in Figure 4e matches with literature results, where a maximum current peak at 0.17 V versus Li/Li^+ (1 M $LiPF_6$ in DMC/EC (50/50 v/v) as electrolyte)[51] and small anodic currents (<0.015 mA·cm^{-2}) below 5.5 V versus Li/Li^+ (1 M $LiPF_6$ in DMC/EC (50/50 v/v))[52] were observed. PVA/CNC membranes show smaller positive and negative peaks around 0 V and similar electrochemical stability at high voltages (see inset in Figure 4e), making them attractive for high-energy cathodes such as $LiNi_{0.5}Mn_{1.5}O_4$ (cutoff voltage of ≈4.7 V versus Li/Li^+),[53] $LiNi_{0.6}Co_{0.2}Mn_{0.2}O_2$ (≈4.3 V versus Li/Li^+),[54] or $Li_3V_2(PO_4)_3$ (4.8 V versus Li/Li^+).[55] In comparison with the intense peaks of 0.578 mA·cm^{-2} for Celgard, a low current of less than 0.15 mA·cm^{-2} at nearly 0 V versus Li/Li^+ for PVA/CNC membranes suggests an even Li plating/stripping onto the working electrodes.

The efficiency of Li^+ deposition is further assessed in symmetric Li/Li cells by performing successive Li plating and stripping cycles at a current density of 0.5 mA·cm^{-2} (**Figure 5**a,b). The over-potential shown by the commercial Celgard separator is considerably larger than the one observed for PVA and PVA/CNC-Li 10 wt% membranes. This over-potential remains well below the 80 mV reported for nano-shielded Celgard separators,[56] or the ≈120 mV achieved for cellulose nanofibers/polyethylene separators.[57] Such low over-potential is a result of the high EU and porous structure of the synthesized separators, facilitating electrolyte infusion and fast Li^+ diffusion between metallic Li and the separator. The voltage oscillations observed when Celgard is used as a separator are indicative of an unstable electrode–separator interface due to poor interfacial compatibility and mechanical detachment of the separator from metallic Li.[58] As shown in Figure 5b, the highly reversible voltage response (no over-potential increase upon cycling) with a polarization square wave after 250 h of plating and stripping indicates a homogeneous Li^+ flux between the electrodes (with no short

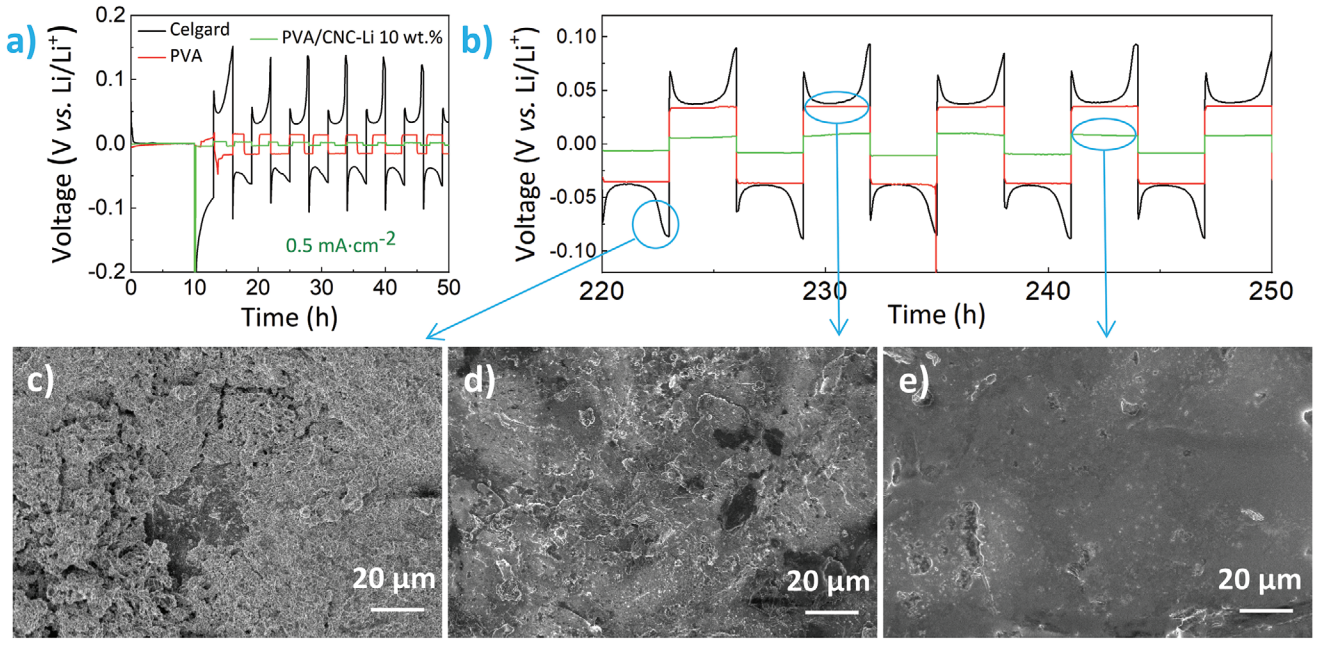

Figure 5. a) Room temperature voltage versus time curves for a Li/Li symmetric cell used for Li plating/stripping at a current density of 0.5 mA·cm^{-2}; b) Magnified view of the voltage versus time curves in the 220–250 h range showing the square wave shape and low polarization of PVA/CNC-Li 10 wt% membrane. Post-mortem SEM micrographs of the Li metal surfaces obtained after galvanostatic cycling at 0.5 mA·cm^{-2} using: c) a Li/Celgard/Li cell; d) Li/PVA/Li cell; and e) Li/PVA/CNC-Li 10 wt%/Li cell soaked in 1 M $LiPF_6$ in DMC/EC (50:50 vol.) as the electrolyte.

circuit) facilitated by the CNCs within the separator-electrolyte pair.[57] Moreover, no degradation in PVA/CNC-Li 10 wt% is observed during cycling (Figure S9, Supporting Information), while the pores of Celgard are completely blocked by Li deposits. Overall, PVA/CNC-Li membranes enable a homogeneous ion transport between the anode and the cathode, guaranteeing an efficient utilization of the active materials.

We also verified if the improved ionic conductivity, Li^+ transport number, stable Li plating/stripping, and interfacial compatibility materializes into a dendrite-free Li deposition. Figure 5c–e shows the SEM images of the Li metal surfaces attained after symmetric galvanostatic cycling. In contrast to the rough morphology obtained in the presence of commercial Celgard, a flat and smooth surface is seen when PVA/CNC-Li 10 wt% is applied as a separator membrane. The highly porous and ionically conducting character of PVA/CNC-Li ensures a stable current flow through the anode-electrolyte interface upon cycling, which in turn yields homogeneous dendrite-free Li deposition.[17]

2.5. Battery Performance

To study the suitability of the PVA/CNC-Li 10 wt% membrane as battery separators (1 M $LiPF_6$ in DMC/EC (50/50 v/v) electrolyte) in a well-known battery system, we chose a standard $LiFePO_4$/Li cell. However, the anodic stability of 5.5 V versus Li/Li^+ of PVA/CNC-Li 10 wt% membranes also allows its use in high-energy 4 V class cathode configurations. The $LiFePO_4$ electrode was fabricated under environmentally friendly conditions, that is, toxic N-methyl-2-pyrrolidone was replaced by water, and as a biodegradable binder we chose polyacrylic acid instead of polyvinylidene fluoride. The first 200 galvanostatic charge/discharge profiles at 100 $mA \cdot g^{-1}$ obtained for commercial Celgard and PVA/CNC-Li 10 wt% membranes are shown in **Figure 6**a,b, respectively. A specific capacity of 106 and 105 $mAh \cdot g^{-1}$ is delivered during the second discharge cycle for Celgard and PVA/CNC-Li 10 wt%, respectively. Cells containing PVA/CNC-Li membranes present a smaller voltage polarization between successive charge/discharge cycles in comparison to Celgard, indicating an improved Li^+ transport between electrodes. As shown in Figure S10 and Table S4, Supporting Information, a reversible capacity of 107 $mAh \cdot g^{-1}$ after 100 cycles results in a gravimetric energy density (cathode only) of 328 $Wh \cdot kg^{-1}$ for the $Li/LiFePO_4$ cell comprising PVA/CNC-Li 10 wt% separator, while 304 $Wh \cdot kg^{-1}$ is achieved for Celgard.

As summarized in Figure 6c, a superior capacity retention of 94 $mAh \cdot g^{-1}$ after 200 cycles is achieved for PVA/CNC-Li 10 wt% membrane in comparison to the 19 $mAh \cdot g^{-1}$ observed for Celgard. In fact, in comparison with Celgard, which suffers a drastic capacity decay after 95 galvanostatic charge/discharge cycles, the PVA/CNC-Li 10 wt% membrane shows a small capacity drop of only 0.04% per cycle. In other words, the excellent electrochemical reversibility enabled by the PVA/CNC-Li 10 wt% membrane allows high capacity retention thanks to its improved Li^+ mobility due to the high ionic conductivity and homogeneous Li^+ flux. Post-mortem morphological analyses of the surface of Li anodes further confirm a dendrite-free homogeneous Li deposition in $Li/LiFePO_4$ cells with PVA/CNC-Li 10 wt% membrane as separator (Figure S11, Supporting Information). Contrarily, the lithium anode from $Li/LiFePO_4$ cells

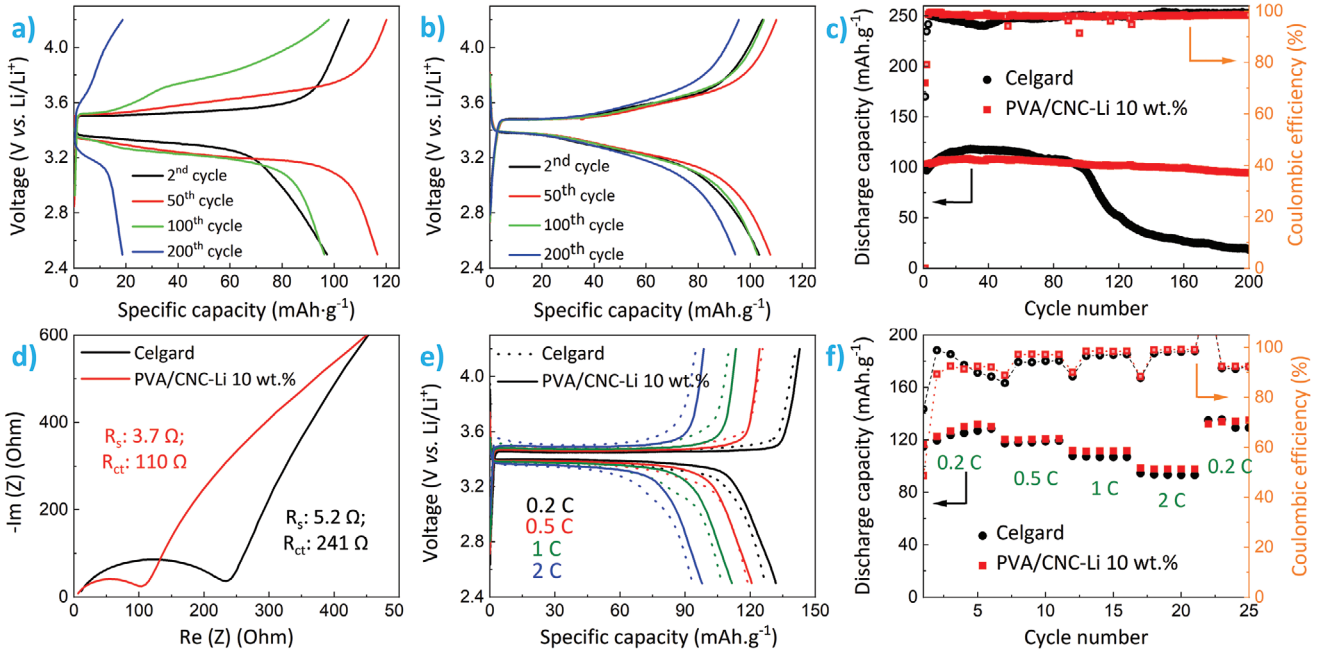

Figure 6. Galvanostatic charge/discharge profiles at 100 $mA \cdot g^{-1}$ in $Li/LiFePO_4$ cells for a) commercial Celgard and b) PVA/CNC-Li 10 wt% as separators soaked in 1 M $LiPF_6$ in DMC/EC (50:50 vol.). c) The corresponding cycling performance (discharge capacity and Coulombic efficiency) during the first 200 cycles. d) EIS spectra of Celgard and PVA/CNC-Li 10 wt% separators obtained after one charging cycle and their corresponding resistances. C-rate performance of both separators: e) galvanostatic charge/discharge profiles and f) C-rate performance.

with Celgard separator presents a rough surface which is characteristic of an inhomogeneous Li^+ deposition upon cycling.

To shed further light on the good capacity retention enabled by PVA/CNC-Li 10 wt% membrane, electrochemical impedance spectra after the first charging cycle in Li/$LiFePO_4$ cells were collected for both Celgard and PVA/CNC-Li 10 wt% membranes. The semicircles in Figure 6d originate from the charge transfer resistance (R_{ct}) at the electrode/electrolyte interface,[59] resulting in an R_{ct} of 110 Ω for PVA/CNC-Li 10 wt% in comparison with 241 Ω for the commercial membrane. Such low resistance, which remains well below the 1506 Ω observed for mesoporous CNC membranes in 1 M $LiPF_6$ in DMC/EC (50:50 vol.),[60] indicates an enhanced interfacial stability between the PVA/CNC-Li 10 wt% membrane and the $LiFePO_4$ cathode, thus yielding an intimate electrolyte/electrode contact.[61] To find out whether or not this low resistance is translated into high rate capability, C-rate performance tests were carried out. As seen in Figure 6e,f, PVA/CNC-Li 10 wt% delivers a higher specific capacity for all the studied rates (0.2, 0.5, 1, and 2 C, where 1 C = 170 mA g^{-1}) with a smaller polarization voltage between the charge/discharge curves (70 mV versus 110 mV at 0.2 C for PVA/CNC-Li 10 wt% versus Celgard), confirming the low charge transport resistance of the membrane comprising lithiated CNCs. Remarkably, the initial capacity is also restored after shifting from 2 C to 0.2 C (fifth cycle: 132 mAh · g^{-1}; 25th cycle: 135 mAh · g^{-1}).

2.6. LIB Transiency Demonstration

The promising electrochemical results for the PVA/CNC-Li membranes and the easily degradable character of the separator encouraged us to investigate their application as transient separators. To exploit the full potential of transiency, the PVA/CNC-Li membranes are soaked into an IL having a butyl-3-methylimidazolium ($Bmim^+$) cation and a $TFSI^-$ anion. Bmim-TFSI was selected because of its adequate combination of ion dissociation ability, relatively low viscosity of 52 cP at 25 °C,[62] relatively high ionic conductivity of 3.9 mS · cm^{-1},[62] biocompatibility, and biodegradability (90% biodegradation after 28 days with *S. paucimobilis* at 45 °C).[63] **Figure 7**a shows the ionic conductivity of IL-soaked membranes obtained from Nyquist impedance measurements at 25 °C (Table S5, Supporting Information). We observe that the ionic conductivity of pure PVA membrane soaked in Bmim-TFSI (0.186 mS · cm^{-1}) is increased up to 0.950 and 0.988 mS · cm^{-1} upon the incorporation of CNCs and lithiated CNCs, respectively (0.171 mS · cm^{-1} for Celgard). In spite of the inherent higher viscosity of the IL hindering an efficient Li^+ diffusion within the porous membrane structure, the ionic conductivity values are above the minimum conductivity of 0.1 mS · cm^{-1} which is usually required for LIB electrolytes. The good values arise from the combination of ions originating from the IL together with the charge carriers provided by the surface of CNCs as a result of ion-exchange processes that yield conductivities even larger than Celgard soaked in aprotic electrolytes.[64] The electrochemical stability of the different membranes infused with Bmim-TFSI is depicted in Figure 7b. The nature of the working electrode significantly influences the oxidation and reduction potentials of ILs. For example, in the presence of stainless steel as working electrodes, ILs undergo undesired reduction/oxidation processes.[65] Therefore, a platinum working electrode was used to determine the electrochemical stability window of the

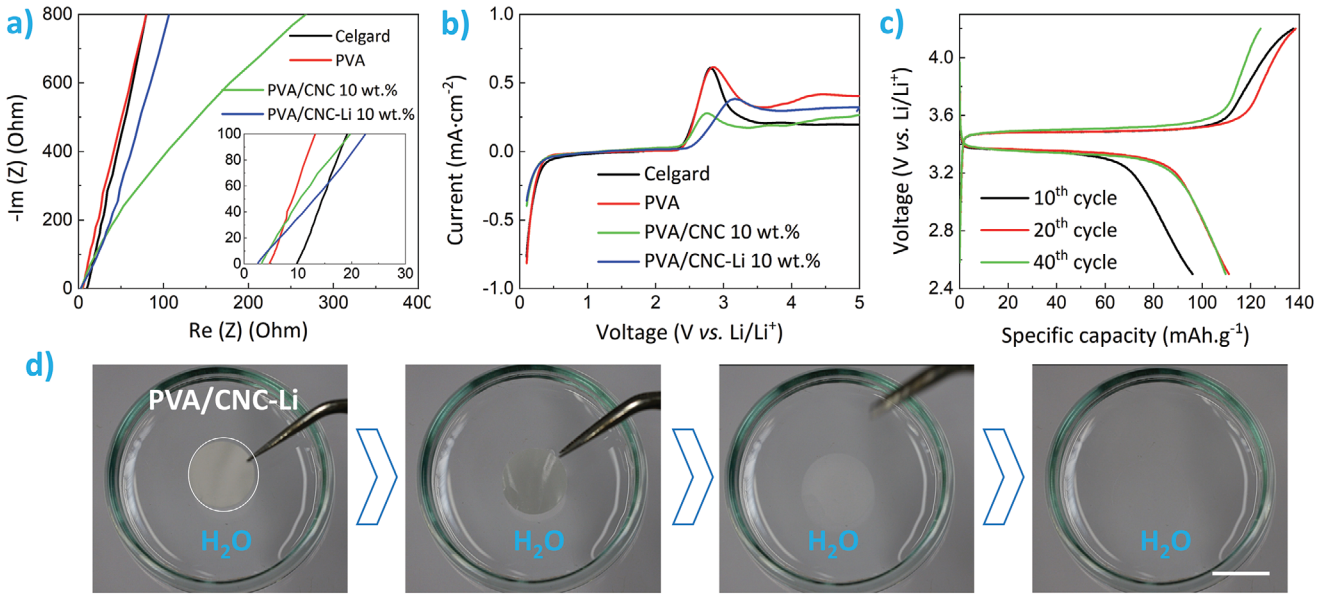

Figure 7. Separators soaked in Bmim-TFSI: a) Nyquist impedance plot showing the intercept of the curve with the real impedance axis, which determines the bulk resistance; and b) electrochemical stability window obtained through linear sweep voltammetry from 0.1 to 5 V with a platinum foil as working electrode and metallic Li as counter electrode at a scan rate of 10 mV · s^{-1}; and c) Galvanostatic charge–discharge profiles at C/10 in Li/$LiFePO_4$ cells for neat PVA/CNC-Li 10 wt% membrane soaked in Bmim-TFSI. d) Optical photographs demonstrating the transiency of a PVA/CNC-Li 10 wt% membrane (∅ = 11 mm) in deionized water at room temperature over a time period of 6 s. The scale bar is 11 mm.

separators soaked in IL.[66] The stability window expands up to 5.0 V versus Li/Li$^+$ similar to other IL-based electrolytes,[67] which is enough for most of the state-of-the-art LIB cathodes. Interestingly, the current increases at 2.5–3.5 V versus Li/Li$^+$, observed for both Celgard and porous PVA membranes, is decreased by the presence of CNCs.

As shown in Figure 7c, PVA/CNC-Li 10 wt% soaked with Bmim-TFSI as separator in a Li/$LiFePO_4$ cell delivers an initial capacity of 96 mAh · g^{-1}, reaching 110 mAh · g^{-1} after 40 cycles at C/10. As shown in Figure S10 and Table S4, Supporting Information, this is translated into a cathode only gravimetric energy density of 70 Wh · kg^{-1} after 100 cycles. For comparison Celgard provides a larger initial capacity of 114 mAh · g^{-1}, but the capacity rapidly decays to 71 mAh · g^{-1} after 40 cycles (Figure S12, Supporting Information). The cycling stability and the unchanged discharge potential plateau indicate that PVA/CNC-Li 10 wt% and Bmim-TFSI are a suitable separator-electrolyte pair for LIBs. Finally, the full transience of the PVA/CNC-Li 10 wt% membrane (∅ = 11 mm) in deionized water within a few seconds is demonstrated in Figure 7d. Such rapid transiency is facilitated by the porous structure and hydrophilicity of the membrane, allowing efficient penetration of water into the whole membrane.

To demonstrate the potential of PVA/CNC-Li membranes for transient energy storage, we fabricate a fully transient rechargeable battery prototype using lithium metal as anode and V_2O_5 nanofibers as cathode (**Figure 8**a). Aluminum (Al) and copper (Cu) tapes were used as current collectors, and the whole battery with a size of 20 × 20 mm was encased in a water-soluble PVA film. V_2O_5 was selected as cathode due to its reversible specific capacity of 294 mAh · g^{-1}, abundance, and low cost.[68] Figure S13, Supporting Information shows the XRD pattern of the synthesized V_2O_5 nanofibers which is consistent with the highly crystalline orthorhombic V_2O_5 phase (Pmmn space group).[68] The electrochemical performance of the transient battery tested in the voltage window of 2.0–4.0 V at a current density of 100 mA · g^{-1} is shown in Figure 8b. The discharge plateaus within the potential window of 3.1 to 3.4 V versus Li indicate a phase transformation of V_2O_5 into $Li_xV_2O_5$.[69] During its second discharge cycle, the battery delivers a capacity of 50 mAh · g^{-1}, which increases to 60 mAh · g^{-1} after 50 cycles and remains stable for 200 cycles (55 mAh · g^{-1}). Such long and stable cycle life with Coulombic efficiencies of nearly 95% is a significant improvement over the performance of degradable batteries previously reported in the literature, which typically operate for just a few hours (24 h for a Mg-Mo battery,[70] 99 h for a Mg-Fe battery)[71] or a few cycles (4 cycles for a Li-V_2O_5 battery,[2] 20 cycles for a LiAl-V_2O_5 battery).[72] The practical relevance of the fully transient rechargeable battery is underlined by the delivered gravimetric energy density of 162 Wh · kg^{-1} (considering the mass of both electrodes) and the stable cycling performance (see Figure S10 and Table S4, Supporting Information).

As seen in Figure 8c, upon immersion in water the battery components fully disappear within 15 min according to:

$$\textit{Anode}: \quad 2Li + 2H_2O \rightarrow 2LiOH + H_2 \tag{1}$$

$$\textit{Cathode}: \quad 2LiOH + V_2O_5 \rightarrow 2LiVO_3 + H_2O \tag{2}$$

$$LiVO_3 + 2LiOH \rightarrow Li_3VO_4 + H_2O \tag{3}$$

$$\textit{Membrane}: \quad \text{Chemical dissolution of PVA + CNC redispersion} \tag{4}$$

$$\textit{Electrolyte}: \quad \text{Chemical dissolution} \tag{5}$$

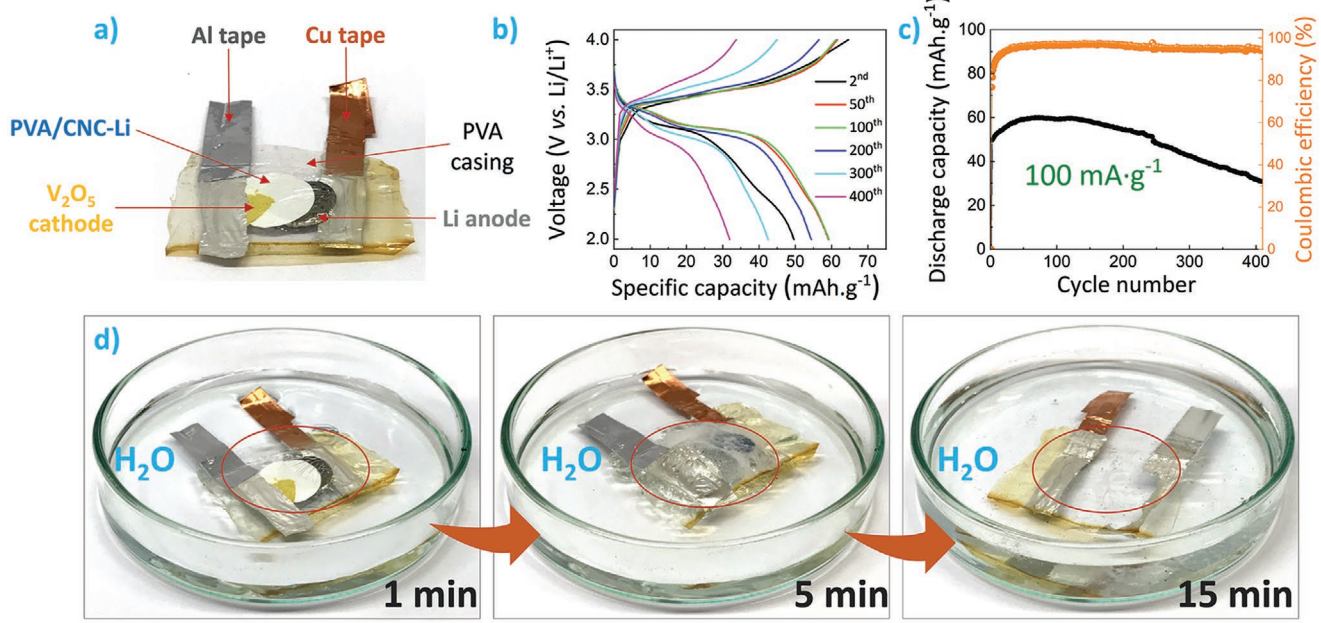

Figure 8. Demonstration of a transient LIB (Li-V_2O_5 system) with PVA/CNC-Li membrane soaked with Bmim-TFSI as separator: a) Optical photograph of the assembled battery; b) galvanostatic charge–discharge profiles at 100 mA·g^{-1}; c) the corresponding cycling performance (discharge capacity and Coulombic efficiency) during the first 400 cycles; and d) optical photographs depicting the dissolution of the transient battery in water over a period of 15 min.

The H_2 gas generated from the reaction of water with the Li anode introduces leaks in the PVA encapsulation, thus enhancing the water diffusion into the battery components and facilitating their prospective dissolution. At the same time, the generated LiOH increases the pH of the water, reacting with the cathode to form colorless and water soluble Li_3VO_4 salt.[2] Simultaneously, the PVA as the main component of the separator fully dissolves in water,[73] while the CNCs form a colloidal solution once their host matrix is removed. In the presence of water, Bmim-TFSI also dissolves given its large Hildebrand's solubility parameter of 22.7–25.4 (at 25 °C).[74] It should be pointed out that the mechanical forces exerted by the H_2 gas release in the form of bubbles break up and disperse non-water soluble components such as CNCs, boosting overall transiency. As a result, the whole battery dissolves within 15 min. In sharp contrast with the conventional LIBs based on petroleum-derived polymers and organic liquid electrolytes, all the components in this battery are readily degraded and mostly identified as non-toxic (Bmim-TFSI presents a median lethal dose LD_{50} of 374 mg · L^{-1} toward fish,[75] while LD_{50} for PVA is as high as 15–20 g · kg^{-1}).[76] However, special care should be taken given the genotoxic character of vanadium oxide, which can result in rhinitis, bronchitis, and pneumonitis.[77] Although some components still need to be replaced with more environmentally friendly alternatives, our work clearly shows that transient batteries are slowly approaching useful electrochemical performance.

3. Conclusions

Here we present a novel strategy for the synthesis of a transient lithium ion conductor with negligible thermal shrinkage and a high transport number using abundant CNCs as additives in a PVA matrix. Upon lithiation and controlled NIPS, the CNCs are selectively located onto the pores of the polymeric membrane. Due to this very specific localization, the $-OSO_3Li$ groups at the surface of the lithiated CNCs are exposed to the electrolyte, resulting in a large amount of mobile Li^+, which in turn provides a remarkable ionic conductivity of 3.077 mS · cm^{-1} and a high Li^+ transport number. The homogeneous Li flux through the membrane as a result of the porous morphology, the high ionic conductivity, and the high cation transport number is translated into a homogeneous and stable Li plating/stripping in a symmetric Li/Li cell, with lower over-potential in comparison with Celgard. These characteristics are materialized into a dendrite-free Li deposition. When assembled in a Li/$LiFePO_4$ cell, a discharge capacity of 94 mAh · g^{-1} at 100 mA · g^{-1} was achieved after 200 cycles. PVA/CNC-Li membranes together with ILs are promising separator-electrolyte pairs that are degradable and biocompatible with high ionic conductivities of up to 0.988 mS · cm^{-1}. The anodic stability of 5.5 V versus Li/Li^+ makes PVA/CNC-Li 10 wt% membranes interesting candidates to high-energy 4 V class cathode configurations. These features make PVA/CNC-Li membranes also attractive for traditional non-transient LIBs to enable longer cycle life batteries. Most importantly, the PVA/CNC-Li membranes can be applied as separator in transient batteries, as exemplified for a Li/V_2O_5 cell, which can operate for over 400 cycles. This prototype of a fully transient battery represents a proof of concept to develop disruptive transient energy storage systems with a long life cycle.

4. Experimental Section

Materials: PVA (M_w: 85.000 – 124.000 g·mol^{-1}, 99+% hydrolyzed (#363146, Sigma Aldrich)) was used as the matrix material for the separator. PVP (K 30) (M_w: 40.000 g·mol^{-1}), microcrystalline cellulose with a particle size of 20 µm (310697-500G), sulfuric acid (95–97%), sodium hydroxide pellets (≥97%), lithium hydroxide monohydrate (>99%), poly(acrylic acid) (M_w: 450.000 g·mol^{-1}), vanadium oxide (V_2O_5) powder (≥99.6%) and hydrogen peroxide (30% w/w) were obtained from Sigma Aldrich. The organic solvent-based electrolyte used was 1 M solution of $LiPF_6$ in DMC/EC (volume ratio 50/50), received from Sigma Aldrich. The IL, 1 butyl-3-methylimidazolium bis(trifluoromethanesulfonyl)imide (Bmim-TFSI, 99.9%) was purchased from Solvionic. Carbon black (Super P) was purchased from TIMCAL Graphite & Carbon. Visking dialysis membranes with a molecular weight cut off of 12.000–14.000 Da were obtained from Medicell Membranes Ltd. For electrochemical studies, 25 µm thick Celgard separators (2325) were used as received.

CNC-Li Synthesis: CNC-Li was prepared in two steps. First, CNCs were prepared by a sulfuric-acid assisted hydrolysis process.[18] 5 g of microcrystalline cellulose was hydrolyzed with 100 mL of 64 wt% sulfuric acid solution at 45 °C for 30 min at a stirring speed of 400 rpm. Hydrolysis was then quenched by adding 1 L of cold deionized water. The excess aqueous acid was removed by centrifugation of the solution at 4000 rpm for 10 min. Water-dispersed colloidal CNCs were achieved by sonication in a Vibracell Sonicator (Sonics & Materials Inc., Danbury, CT) at 40% output for 5 min. This process was a common approach for CNCs preparation, wherein water-dispersed CNCs were decorated with sulfate half-ester groups (pH of 2.3, 1.16 wt% concentration).

Sulfated CNCs were then lithiated through a reaction with LiOH solution to obtain CNC-Li. Water-dispersed CNCs were desulfated using a 7 wt% NaOH solution at 65 °C for 5 h.[78] After thoroughly washing with water to remove the excess of NaOH, LiOH was added to the water-dispersed CNCs to obtain a 2 M aqueous colloidal solution. Lithiation was conducted over 24 h at RT. CNCs were then washed several times with deionized water. An additional purification step involving dialysis against distilled water for 7 days using a Visking membrane was carried out. Finally, the aqueous CNC-Li dispersion was tip-sonicated at 40% output for 5 min to ensure a homogeneous dispersion. The colloidal CNC-Li with 2.32 wt% concentration was stored in the fridge at 4 °C until needed.

Fabrication of Porous PVA-Based Membranes: As summarized in **Scheme 1**, porous PVA/CNC and PVA/CNC-Li separators with nanocrystal concentrations of 0, 1, 3, 5, and 10 wt% (with respect to PVA) were prepared following a modified NIPS wet-process method,[24] wherein PVP was used as a pore-forming agent. First, a solution of PVA and PVP was prepared by mixing 1000 mg of PVP with different amounts of PVA (from 900 to 1000 mg) in water at 90 °C for 2.5 h (see Table S1, Supporting Information for specific formulation). After 2.5 h of mixing, the solution was cooled down to 50 °C to prevent degradation of CNC or CNC-Li. A given amount of CNC (or CNC-Li) was added to the PVA/PVP solution and then mixed with a spatula for a few minutes followed by magnetic stirring for the next 30 min. The resulting dispersion was then stored at room temperature overnight to reach thermal equilibrium and to remove air bubbles.

The homogenous solution/dispersion was stirred again for 30 min at 30 °C using a magnetic stirrer. A centrifugation step at 4000 rpm for 5 min was performed to remove any air bubbles and undissolved material. The solution/dispersion was then cooled to 6 °C in an ice/ethanol bath. At such low temperature, the presence of more crystalline microdomains in PVA help to achieve a porous structure.[79] The solution/dispersion was then directly cast onto a clean glass substrate

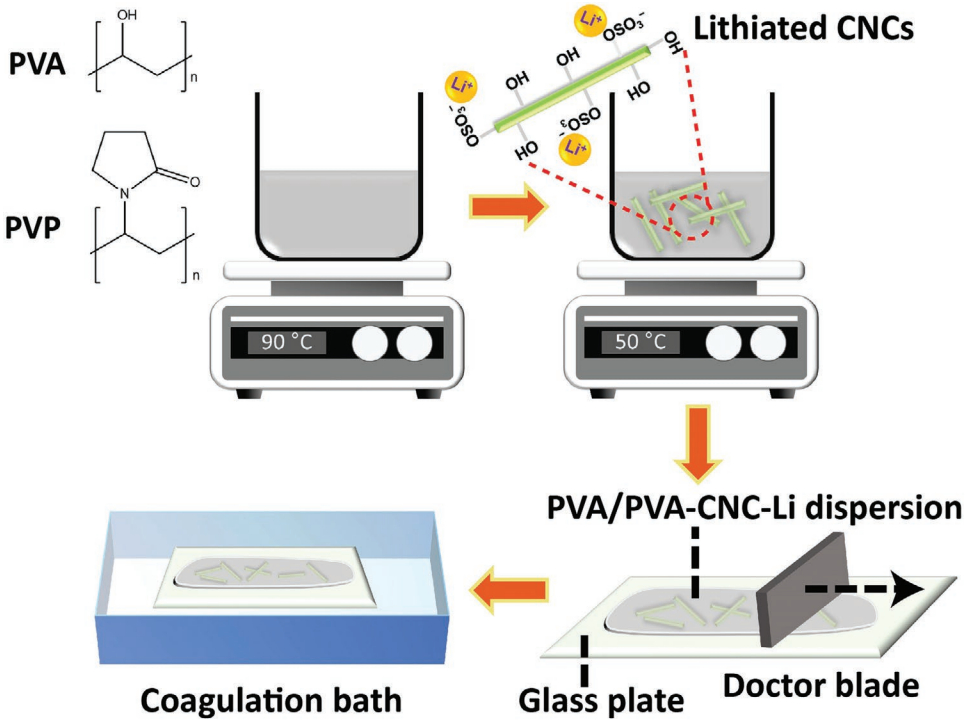

Scheme 1. Schematic representation showing the fabrication process of PVA/CNC-Li membranes.

using a Doctor blade system with a 150 µm gap (the distance between the glass plate and blade itself) followed by immersion into an ethanol coagulation bath at room temperature for 4 h. The film was carefully removed from the bath, transferred to a Teflon plate, and vacuum dried. It was noticed that vacuum drying was an essential step to obtain porous membranes, as drying under ambient conditions resulted in transparent and comparably dense films (Figure S1, Supporting Information).

Supporting Information

Supporting Information is available from the Wiley Online Library or from the author.

Acknowledgements

The authors gratefully acknowledge financial support from ETH Zurich (ETH Research Grant ETH-45 18-1). The authors thank Medicell Membranes Ltd. for kindly providing Visking dialysis membranes. The authors acknowledge support from the Scientific Center for Optical and Electron Microscopy (ScopeM) of ETH Zurich. The authors also thank Dr. Dipan Kundu for helpful discussions on transport number.

Conflict of Interest

The authors declare no conflict of interest.

Data Availability Statement

Research data are not shared.

Keywords

cellulose nanocrystals, degradation, ionic liquids, lithium ion batteries, sustainability, transiency

Received: March 22, 2021
Revised: May 6, 2021
Published online: June 16, 2021

[1] S.-W. Hwang, H. Tao, D.-H. Kim, H. Cheng, J.-K. Song, E. Rill, M. A. Brenckle, B. Panilaitis, S. M. Won, Y.-S. Kim, Y. M. Song, K. J. Yu, A. Ameen, R. Li, Y. Su, M. Yang, D. L. Kaplan, M. R. Zakin, M. J. Slepian, Y. Huang, F. G. Omenetto, J. A. Rogers, *Science* **2012**, *337*, 1640.
[2] K. Fu, Z. Liu, Y. Yao, Z. Wang, B. Zhao, W. Luo, J. Dai, S. D. Lacey, L. Zhou, F. Shen, M. Kim, L. Swafford, L. Sengupta, L. Hu, *Nano Lett.* **2015**, *15*, 4664.
[3] N. Mittal, A. Ojanguren, M. Niederberger, E. Lizundia, *Adv. Sci.* **2021**, 2004814.
[4] C. Liu, J. Lin, H. Cao, Y. Zhang, Z. Sun, *J. Cleaner Prod.* **2019**, *228*, 801.
[5] United Nations, https://sdgs.un.org/2030agenda (accessed: February 2021).
[6] E. Lizundia, D. Kundu, *Adv. Funct. Mater.* **2020**, *31*, 2005646.
[7] P. Arora, Z. Zhang, *Chem. Rev.* **2004**, *104*, 4419.
[8] Y. Gao, Y. Zhang, X. Wang, K. Sim, J. Liu, J. Chen, X. Feng, H. Xu, C. Yu, *Sci. Adv.* **2017**, *3*, e1701222.
[9] S.-W. Hwang, S.-K. Kang, X. Huang, M. A. Brenckle, F. G. Omenetto, J. A. Rogers, *Adv. Mater.* **2015**, *27*, 47.
[10] Y. He, X. Ren, Y. Xu, M. H. Engelhard, X. Li, J. Xiao, J. Liu, J.-G. Zhang, W. Xu, C. Wang, *Nat. Nanotechnol.* **2019**, *14*, 1042.

[11] H. Zhang, C. Li, M. Piszcz, E. Coya, T. Rojo, L. M. Rodriguez-Martinez, M. Armand, Z. Zhou, *Chem. Soc. Rev.* **2017**, *46*, 797.
[12] L. Porcarelli, A. S. Shaplov, F. Bella, J. R. Nair, D. Mecerreyes, C. Gerbaldi, *ACS Energy Lett.* **2016**, *1*, 678.
[13] Q. Ma, H. Zhang, C. Zhou, L. Zheng, P. Cheng, J. Nie, W. Feng, Y.-S. Hu, H. Li, X. Huang, L. Chen, M. Armand, Z. Zhou, *Angew. Chem., Int. Ed.* **2016**, *55*, 2521.
[14] L. Meabe, N. Goujon, C. Li, M. Armand, M. Forsyth, D. Mecerreyes, *Batteries Supercaps* **2020**, *3*, 68.
[15] G. Homann, L. Stolz, J. Nair, I. C. Laskovic, M. Winter, J. Kasnatscheew, *Sci. Rep.* **2020**, *10*, 4390.
[16] H. Zhang, F. Chen, O. Lakuntza, U. Oteo, L. Qiao, M. Martinez-Ibañez, H. Zhu, J. Carrasco, M. Forsyth, M. Armand, *Angew. Chem., Int. Ed.* **2019**, *58*, 12070.
[17] C. Hänsel, E. Lizundia, D. Kundu, *ACS Appl. Energy Mater.* **2019**, *2*, 5686.
[18] E. Lizundia, D. Puglia, T.-D. Nguyen, I. Armentano, *Prog. Mater. Sci.* **2020**, *112*, 100668.
[19] K. Shi, X. Yang, E. D. Cranston, I. Zhitomirsky, *Adv. Funct. Mater.* **2016**, *26*, 6437.
[20] R. Pan, R. Sun, Z. Wang, J. Lindh, K. Edström, M. Strømme, L. Nyholm, *Energy Storage Mater.* **2019**, *21*, 464.
[21] Q. Huang, J. Song, Y. Gao, D. Wang, S. Liu, S. Peng, C. Usher, A. Goliaszewski, D. Wang, *Nat. Commun.* **2019**, *10*, 5586.
[22] Q. Bai, G. Zhang, B. Xu, X. Feng, H. Jiang, H. Li, *RSC Adv.* **2015**, *5*, 91213.
[23] W. Xiao, L. Zhao, Y. Gong, J. Liu, C. Yan, *J. Membr. Sci.* **2015**, *487*, 221.
[24] W. Xiao, K. Zhang, J. Liu, C. Yan, *J. Mater. Sci.: Mater. Electron.* **2017**, *28*, 17516.
[25] P. V. Chombo, Y. Laoonual, *J. Power Sources* **2020**, *478*, 228649.
[26] X. Feng, M. Ouyang, X. Liu, L. Lu, Y. Xia, X. He, *Energy Storage Mater.* **2018**, *10*, 246.
[27] A. Lejardi, A. Etxeberria, E. Meaurio, J.-R. Sarasua, *Polymer* **2012**, *53*, 50.
[28] U. Goikuria, A. Larrañaga, J. L. Vilas, E. Lizundia, *Carbohydr. Polym.* **2017**, *171*, 193.
[29] C. Hänsel, D. Kundu, *ACS Omega* **2019**, *4*, 2684.
[30] M. Forsyth, L. Porcarelli, X. Wang, N. Goujon, D. Mecerreyes, *Acc. Chem. Res.* **2019**, *52*, 686.
[31] X. Wang, F. Chen, G. M. A. Girard, H. Zhu, D. R. MacFarlane, D. Mecerreyes, M. Armand, P. C. Howlett, M. Forsyth, *Joule* **2019**, *3*, 2687.
[32] X. Jia, C. Wang, V. Ranganathan, B. Napier, C. Yu, Y. Chao, M. Forsyth, F. G. Omenetto, D. R. MacFarlane, G. G. Wallace, *ACS Energy Lett.* **2017**, *2*, 831.
[33] S. Yamada, H. Toshiyoshi, *Small* **2018**, *14*, 1800937.
[34] S. Y. Oh, D. Il Yoo, Y. Shin, H. C. Kim, H. Y. Kim, Y. S. Chung, W. H. Park, J. H. Youk, *Carbohydr. Res.* **2005**, *340*, 2376.
[35] A. Kharazmi, N. Faraji, R. Mat Hussin, E. Saion, W. M. M. Yunus, K. Behzad, *Beilstein J. Nanotechnol.* **2015**, *6*, 529.
[36] P. Liu, W. Chen, C. Liu, M. Tian, P. Liu, *Sci. Rep.* **2019**, *9*, 9534.
[37] V. Heshmati, M. R. Kamal, B. D. Favis, *Eur. Polym. J.* **2018**, *98*, 11.
[38] L. Frenck, G. K. Sethi, J. A. Maslyn, N. P. Balsara, *Front. Energy Res.* **2019**, *7*, 115.
[39] S. Cui, L. Li, Q. Wang, *Compos. Sci. Technol.* **2016**, *127*, 177.
[40] B. Xiong, R. Chen, F. Zeng, J. Kang, Y. Men, *J. Membr. Sci.* **2018**, *545*, 213.
[41] X. Casas, M. Niederberger, E. Lizundia, *ACS Appl. Mater. Interfaces* **2020**, *12*, 29264.
[42] S. J. Chun, E. S. Choi, E. H. Lee, J. H. Kim, S. Y. Lee, S. Y. Lee, *J. Mater. Chem.* **2012**, *22*, 16618.
[43] J.-M. Kim, C. Kim, S. Yoo, J.-H. Kim, J.-H. Kim, J.-M. Lim, S. Park, S.-Y. Lee, *J. Mater. Chem. A* **2015**, *3*, 10687.
[44] T.-W. Zhang, J.-L. Chen, T. Tian, B. Shen, Y.-D. Peng, Y.-H. Song, B. Jiang, L.-L. Lu, H.-B. Yao, S.-H. Yu, *Adv. Funct. Mater.* **2019**, *29*, 1902023.
[45] J. Evans, C. A. Vincent, P. G. Bruce, *Polymer* **1987**, *28*, 2324.
[46] D. M. Pesko, K. Timachova, R. Bhattacharya, M. C. Smith, I. Villaluenga, J. Newman, N. P. Balsara, *J. Electrochem. Soc.* **2017**, *164*, E3569.
[47] D. T. Hallinan, I. Villaluenga, N. P. Balsara, *MRS Bull.* **2018**, *43*, 759.
[48] J. Mindemark, M. J. Lacey, T. Bowden, D. Brandell, *Prog. Polym. Sci.* **2018**, *81*, 114.
[49] P. G. Bruce, M. T. Hardgrave, C. A. Vincent, *Solid State Ionics* **1992**, *53*, 1087.
[50] Q. Li, J. Chen, L. Fan, X. Kong, Y. Lu, *Green Energy Environ.* **2016**, *1*, 18.
[51] Y. Zhu, J. Cao, H. Chen, Q. Yu, B. Li, *J. Mater. Chem. A* **2019**, *7*, 6832.
[52] W. Shen, K. Li, Y. Lv, T. Xu, D. Wei, Z. Liu, *Adv. Energy Mater.* **2020**, *10*, 1904281.
[53] X. Xu, S. Lee, S. Jeong, Y. Kim, J. Cho, *Mater. Today* **2013**, *16*, 487.
[54] G. Salitra, E. Markevich, M. Afri, Y. Talyosef, P. Hartmann, J. Kulisch, Y.-K. Sun, D. Aurbach, *ACS Appl. Mater. Interfaces* **2018**, *10*, 19773.
[55] Q. Ni, L. Zheng, Y. Bai, T. Liu, H. Ren, H. Xu, C. Wu, J. Lu, *ACS Energy Lett.* **2020**, *5*, 1763.
[56] Z. J. Liang, Q. Chen, X. Liao, P. Yao, B. Zhu, G. Lv, X. Wang, X. Chen, J. Zhu, *Angew. Chem., Int. Ed.* **2020**, *59*, 6561.
[57] R. Pan, X. Xu, R. Sun, Z. Wang, J. Lindh, K. Edström, M. Strømme, L. Nyholm, *Small* **2018**, *14*, 1704371.
[58] S. Xia, J. Lopez, C. Liang, Z. Zhang, Z. Bao, Y. Cui, W. Liu, *Adv. Sci.* **2019**, *6*, 1802353.
[59] W. Choi, H.-C. Shin, J. M. Kim, J.-Y. Choi, W.-S. Yoon, *J. Electrochem. Sci. Technol.* **2020**, *11*, 1.
[60] G. G. Eshetu, G. A. Elia, M. Armand, M. Forsyth, S. Komaba, T. Rojo, S. Passerini, *Adv. Energy Mater.* **2020**, *10*, 2000093.
[61] A. Barai, G. H. Chouchelamane, Y. Guo, A. McGordon, P. Jennings, *J. Power Sources* **2015**, *280*, 74.
[62] M. Vranes, S. Dozic, V. Djeric, S. Gadzuric, *J. Chem. Eng. Data* **2012**, *57*, 1072.
[63] C. Abrusci, J. Palomar, J. L. Pablos, F. Rodriguez, F. Catalina, *Green Chem.* **2011**, *13*, 709.
[64] L. Guerreiro da Trindade, M. R. Becker, F. Celso, C. L. Petzhold, E. M. A. Martini, R. F. de Souza, *Polym. Eng. Sci.* **2016**, *56*, 1037.
[65] M. Galiński, A. Lewandowski, I. Stepniak, *Electrochim. Acta* **2006**, *51*, 5567.
[66] Z. Xue, L. Qin, J. Jiang, T. Mu, G. Gao, *Phys. Chem. Chem. Phys.* **2018**, *20*, 8382.
[67] J. R. Nair, F. Colò, A. Kazzazi, M. Moreno, D. Bresser, R. Lin, F. Bella, G. Meligrana, S. Fantini, E. Simonetti, G. B. Appetecchi, S. Passerini, C. Gerbaldi, *J. Power Sources* **2019**, *412*, 398.
[68] E. Brown, J. Acharya, G. P. Pandey, J. Wu, J. Li, *Adv. Mater. Interfaces* **2016**, *3*, 1600824.
[69] M. L. Divya, S. Natarajan, Y.-S. Lee, V. Aravindan, *Small* **2020**, *16*, 2002624.
[70] L. Yin, X. Huang, H. Xu, Y. Zhang, J. Lam, J. Cheng, J. A. Rogers, *Adv. Mater.* **2014**, *26*, 3879.
[71] M. Tsang, A. Armutlulu, A. W. Martinez, S. A. B. Allen, M. G. Allen, *Microsyst. Nanoeng.* **2015**, *1*, 15024.
[72] K. Fu, Z. Wang, C. Yan, Z. Liu, Y. Yao, J. Dai, E. Hitz, Y. Wang, W. Luo, Y. Chen, M. Kim, L. Hu, *Adv. Energy Mater.* **2016**, *6*, 1502496.
[73] E. Chiellini, A. Corti, S. D'Antone, R. Solaro, *Prog. Polym. Sci.* **2003**, *28*, 963.
[74] A. Marciniak, *Int. J. Mol. Sci.* **2010**, *11*, 1973.
[75] M. El-Harbawi, *Procedia Chem.* **2014**, *9*, 40.
[76] C. C. DeMerlis, D. R. Schoneker, *Food Chem. Toxicol.* **2003**, *41*, 319.
[77] A. Kulkarni, G. S. Kumar, J. Kaur, K. Tikoo, *Inhalation Toxicol.* **2014**, *26*, 772.
[78] T. Fujisaki, K. Kashima, S. Serrano-Luginbühl, R. Kissner, D. Bajuk-Bogdanović, M. Milojević-Rakić, G. Ćirić-Marjanović, S. Busato, E. Lizundia, P. Walde, *RSC Adv.* **2019**, *9*, 33080.
[79] S. Huang, F. Wan, S. Bi, J. Zhu, Z. Niu, J. Chen, *Angew. Chem., Int. Ed.* **2019**, *58*, 4313.